High field physics and extreme nonlinear optics

Brilliance measurement of high order harmonic generation

S.M. Teichmann[1,a], N. Bisht[2], M. Hidalgo[3], A. Honarfar[4], M.G. Mingolla[5], M. Turconi[6], M. Clerici[3], P. Di Trapani[7], and J. Biegert[1,8]

[1] ICFO-Institut de Ciencies Fotoniques, Mediterranean Technology Park, 08860 Castelldefels (Barcelona), Spain
[2] National Physical Laboratory, 110012 New Delhi, India
[3] INRS-EMT, Université du Québec, Varennes, Québec J3X 1S2, Canada
[4] Laser and Plasma Institute, Shahid Beheshti University, Evin, Tehran, Iran
[5] INRIM, Torino 10135, Italy
[6] INLN, Sophia Antipolis, 06560 Valbonne, France
[7] Department of Physics and Mathematics, University of Insubria at Como, 22100 Como, Italy
[8] ICREA-Institució Catalana de Recercea i Estudis Avançats, 08010 Barcelona, Spain

Abstract. Despite the fact that high order harmonic generation (HHG) aims at serving as a table-top light source for imaging applications with extremely high spatial resolution, a general lack of accurate conversion efficiency measurements exists in the field. Here, we present such a measurement for a HHG setup with a semi-infinite gas cell. By combining measurements with a calibrated photodiode sensitive in the extreme ultra-violet (XUV) and spatially resolved spectral measurements of HHG spectra, we are able to determine conversion efficiencies of the HHG process as well as brilliance values for individual harmonics. The method is explained in detail and applicable to any target geometry.

1 Introduction

Dynamics of electrons is centerpiece to most processes in nature and determines, e.g., chemical reaction dynamics, charge motion in photosynthesis, or biochemical reactions and protein folding. It is therefore of paramount interest to study electronic motion at its natural time scale, which is on the order of the atomic unit of time $\tau_{at} = 24\,\mathrm{as}$, where $1\,\mathrm{as} = 10^{-18}\,\mathrm{s}$. Resolving electron dynamics temporally therefore necessitates the generation of probing mechanisms on the as-timescale. Ultrashort light pulses with as-duration satisfy this condition and have thus received significant attention in the scientific community in the past decade.

[a] e-mail: stephan.teichmann@icfo.es

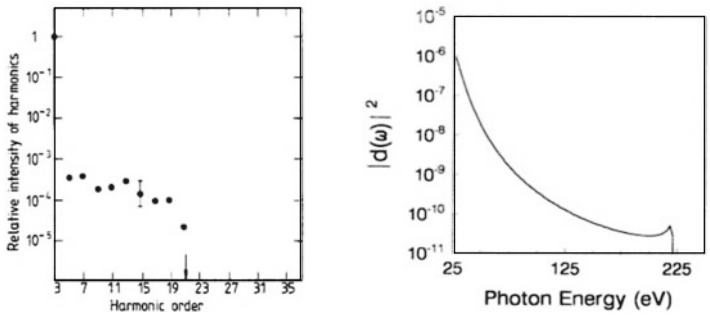

Fig. 1. Left: one of the first HHG measurements, generated in xenon gas with a fundamental of 1064 nm. It clearly shows the characteristic features of the plateau region and the sharp cut-off which were explained some years later by the three-step model. Figure taken from [2]. Right: calculation with the three-step model, reproducing the plateau and cut-off of a HHG spectrum. Plotted is the absolute square of the dipole moment (proportional to the harmonic signal) vs. the emitted photon energy, calculated for 1064 nm radiation interacting with helium. Figure taken from [4].

Light pulses on the as-time scale inherently necessitate a short carrier wavelength: For a light pulse to propagate, its duration must at least equal one cycle duration of its carrier frequency. Extensive effort has been put into the development of short wavelength-, short pulse duration-sources: Synchrotrons provide very intense, yet temporally incoherent radiation reaching even beyond the XUV range (between 120 nm and 10 nm), while their pulse duration is at best several hundred picosecond ($1\,\mathrm{ps} = 10^{-12}\,\mathrm{s}$). Another source of XUV and SXR light (the SXR range lies between 10 nm and 0.1nm), which has recently regained interest is the free electron laser. Such sources however are based on amplified spontaneous emission and are currently limited by the fact that emission is random.

Naturally, great effort has been placed into the development of fully coherent, laser-like sources of XUV and SXR light which are compact enough to be accommodated in research and production laboratories. A solution is given by the radiation resulting from the interaction of highly intense laser light with a nonlinear medium, termed high harmonic generation (HHG). As shall be discussed below and in Sect. 2, radiation from HHG takes on the coherence of its generating laser light, can be emitted in pulses of sub-fs duration and spectrally extends into the XUV regime.

HHG as an XUV source. The first experimental demonstration of the generation of higher order harmonics was shown in 1987 with a KrF^* laser at 248 nm [1] and in 1988 with a Nd:YAG laser at 1064 nm [2,3]. These experiments, though limited in peak intensity and thus to a highest harmonic order of 33, proved the feasibility of HHG and showed characteristic features, as shown in the left plot in Fig. 1. These features were theoretically described for the first time by semiclassical models in 1993 [4,5], deepening the understanding of HHG. At the same time, chirped-pulse-amplified Ti:Sapphire were developed [6], making higher intensities readily available. Together, these developments paved the way for a new research field.

Attoscience. With the general theory of HHG introduced in 1993 and high intensity Ti:Sapphire laser systems readily available, increasingly high orders of harmonics were generated. Advances in the field of the temporal characterization of sub-fs pulse durations in combination with the increased bandwidth due to HHG led to the first measurement of pulses with as-duration in 2001 [7]. Shortly after, a first

proof-of-principle experiment demonstrated the measurement of sub-fs relaxation dynamics of core-excited atoms [8], marking the beginning of a new field of research termed Attoscience [9–12].

Characterizing HHG. Besides temporally resolved measurements of ultrafast dynamics in atomic and molecular systems, the spatial coherence of HHG radiation promises great potential for imaging applications with very high spatial resolution. However, as shall be discussed below, an inherent drawback of the process of HHG in this regard is its low yield of XUV photons, in particular with respect to synchrotrons and free electron lasers as alternatives. The aim of this research project is to characterize the yield of the HHG process for a particular target configuration and hence to relate the performance of the source to its intended application.

2 Theoretical background

Beyond laser intensities of $10^{13}\,\mathrm{W/cm^2}$, the electric field E_0 of a laser pulse can have a significant effect on the electric binding field in an atom such that the non-perturbative regime is reached. In this section we discuss how the interaction of such strong laser fields with matter can lead to HHG and introduce the physics of the proposed project.

The Three-Step Model. To introduce the theory of HHG, we shall begin by considering a semi-classical model of a single atom interacting with an intense laser pulse [4,5]. The electric field E_0 of the laser pulse can distort the atomic potential sufficiently for valence electrons to have a finite probability of tunneling into the continuum (step 1). Once released into the continuum, the force on the electron due to the laser field significantly exceeds the Coulomb force by the parent ion so that it can be approximated as interacting freely with the laser field. By following the oscillating electric field the electron gains kinetic energy (step 2) through the ponderomotive potential of the laser field: $\mathrm{U}_p \propto E_0^2$. If the laser field is linearly polarised, there is a finite probability of the electron re-colliding with the atom (step 3). In this last step, the gained kinetic energy plus the ionization potential I_p can be released as highly energetic photons, leading to a maximal photon energy of $3.2\,\mathrm{U}_p + \mathrm{I}_p$ which is known as the *cut-off*.

Interestingly, the harmonic orders below the cut-off form an intensity *plateau* when plotted on a logarithmic scale, shown in Fig. 1. It required the three-step model to explain this effect: The release mechanism is not a multi-photon process but tunnel ionization and therefore the response does not follow the inverse power law known from perturbative nonlinear frequency conversion processes.

The Quantum Mechanical Picture. Some details of the HHG process can only be revealed by treating the extreme light-matter interaction quantum mechanically [13,14]. Assigning a wavefunction $|\psi(t)\rangle$ to the electron, its dipole moment is given by $\mathbf{D}(t) = \langle\psi(t)|\mathbf{x}|\psi(t)\rangle$. The emitted radiation is proportional to the acceleration of $\mathbf{D}(t)$, *i.e.* $\ddot{\mathbf{D}}(t)$, where the wavefunction $|\psi(t)\rangle$ is obtained by solving the time-dependent Schrödinger equation. It is important to note that when considering the effect of only one electron excursion, the emitted radiation is continuous. However, the process is repeated every half-cycle, given that the electric field strength is sufficient to cause tunnel ionization, and this periodicity in the time domain leads to the generation of odd harmonic orders in the frequency domain. Finally, since the source of the fully

deterministic process of HHG is temporally and spectrally coherent laser light, these properties are mapped onto the resulting XUV radiation.

The Single Atom Response Yield. As indicated in the previous paragraph, the signal strength of the radiation emitted by a single atom significantly depends on the electron wavefunction. It is instructive to relate the properties of this wavefunction to experimental parameters when discussing the efficiency of the HHG process on the single atom level.

Generally, the yield of HHG is determined by the interplay of two probabilites. The higher the intensity of the driving laser pulse, the higher is the probability for the electron to tunnel ionise into the continuum state due to greater distortion of the Coulomb potential. On the contrary, the probability of the electron recombining with the parent ion decreases with increasing intensity due to an icreased spreading of the electron wavepacket [15]. Hence, even on the microscopic level it is not necessarily beneficial to simply increase the intensity of the driving laser pulse. We conclude that the driving intensity is a crucial parameter to observe when analyzing the HHG efficiency.

The Macroscopic Response. So far, we have only considered the single atom response of the HHG process. However, for a complete picture of HHG it is essential to consider the interaction of a laser pulse with an ensemble of atoms, i.e. with a macroscopic target. Fundamentally, the macroscopic response is the coherent superposition of the single atom response at different positions and at different times in the target. Practically, this is always the measured quantity since (1) it is difficult to produce single-atom targets and (2) the response of such a target would be too weak to detect.

Any nonlinear optical process, and thus also HHG, requires a constant phase relation between the generating and generated waves throughout the interaction region [16] which is commonly known as *phase-matching*. Only if this is satisfied can the generated waves emitted by atoms at different positions in the target interfere constructively. Various inherent properties of HHG, such as dispersion, free electron production and an intrinsic phase of the HHG process, lead to a considerable phase mismatch between the fundamental and its higher harmonic orders [17]. This poses a limitation to the overall efficiency of HHG.

Another limiting factor regarding the yield of HHG is reabsorption of the XUV radiation. The combination of interaction length and target gas pressure determine whether the generated higher oder harmonics actually escape the target or if they are reabsorbed [18].

Phase-Matching and Absorption. The phase relation between the laser-driven single atom response and the propagating harmonics is expressed as Δk. For a given interaction length, the frequency conversion process is considered *phase-mismatched* when $\Delta k \neq 0$. In this case the harmonics emitted at different positions in the interaction region are out of phase so that they cannot interfere constructively. Consequently, the efficiency in this configuration is lower compared to the *phase-matched* case of $\Delta k = 0$. This paragraph shall highlight which experimental parameters determine the phase-matching conditions.

As a first approximation, the phase-mismatch between the fundamental and the harmonic radiation can be separated into three contributions: $\Delta k = \Delta k_{geom} + \Delta k_{disp} + \Delta k_{ion}$. The first term, Δk_{geom}, is determined by the confinement of the driving laser pulse which leads to a retardation of its phase relative to its free propagation. Due to their much smaller wavelengths, the harmonics are not affected by the confinement, so that this term generally gives a negative contribution to Δk.

The dispersion term Δk_{disp} arises from different phase velocities of the fundamental and harmonic radiation in the target gas. From the proportionality $\Delta k_{disp} \propto qP\Delta n$ we see that it depends on the harmonic order q, the gas pressure P as well as the difference in the refractive indices Δn, at the laser and the harmonic wavelengths. Since the refractive index is larger at longer wavelengths, the dispersion contribution to Δk is positive. Finally, the ionization term $\Delta k_{ion} \propto -qP\eta$, where η is the fraction of ionized atoms, describes how the free electrons resulting from the ionization of the gas medium affect phase-matching. The created plasma reduces the refractive index more strongly for the laser than for the harmonics so that its overall contribution is always negative.

It is obvious that phase-matching is reached when the negative geometric and ionization terms cancel out the positive dispersion term, satisfying the condition $\Delta k = 0$. However, even if this is achieved, the harmonic signal does not grow limitless when extending the interaction length to very large values. We rather find the case of *absorption-limited* harmonics, meaning that the overall signal strength is limited by the reabsorption of the harmonics by the target gas. Quantitatively, this can be expressed in terms of the absorption coefficient $\alpha = Pd_0\sigma/2$ where d_0 is the gas number density and σ is the absorption cross section of an atom.

HHG Efficiency Measurement. From this brief discussion of single atom response, phase-matching and absorption parameters we can draw important conclusions for HHG efficiency measurements. Both the microscopic and the macroscopic pictures suggest that simply driving the system harder, i.e. with a higher intensity, does not directly lead to a higher harmonic signal. Microscopically, this is due to the recombination probability while macroscopically the ionization fraction hinders phase-matching. Furthermore, we understand that the target gas pressure is a valuable parameter to adjust with respect to the signal as it influences both phase-matching as well as absorption. Consequently, a scan of the laser pulse intensity, the gas pressure as well as the propagation distance of the harmonics in neutral gas is of crucial importance during the experiment.

3 Experimental setup

In this project we intend to measure experimentally not only the efficiency of the HHG process but also its brilliance.The fundamental approach is to measure the energy in a generated pulse of harmonics as well as its spectral and angular content, giving us the opportunity to determine both desired quantities. We shall do this for a particular target geometry (see below) which has not been performed so far, thus extending the detailed analysis of HHG configurations.

Experimental setup. We intend to keep the experimental setup simple and reliable, yet allowing for accurate HHG yield measurements. A coarse schematic of the setup indicating the main components is shown in Fig. 2. The output of an amplified Ti:Sapphire laser system is focused into a semi-infinite gas cell [19] which can be filled with different rare gases to pressures of about 300 mbar. This cell is covered with a removable lid so that the inside can be accessed at will. A pinhole terminates the semi-infinite gas cell and primarily serves as a pumping aperture to the analyzer chamber. Inside the analyzer chamber are an adjustable slit as well as an XUV flat-field spectrometer. The latter consists of a reflective diffraction grating (Hitachi) and an MCP with a fluorescent back-screen (Hamamatsu) whose signal is imaged onto a CCD chip. This setup allows us to resolve the HHG signal spectrally as well as spatially, as indicated in the schematic.

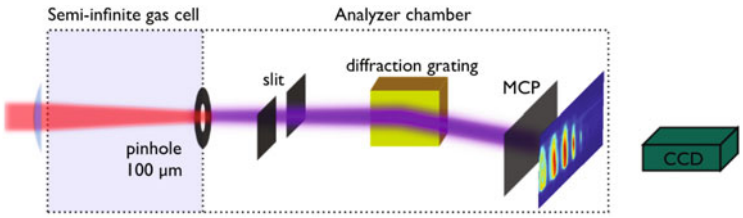

Fig. 2. Schematic of the experimental setup (not to scale).

Not shown in the schematic is an XUV sensitive photodiode which we shall use for the energy measurement of the generated harmonics. To distinguish the XUV photons from radiation of the driving laser, we introduce aluminium filters of 500 nm thickness. Their transmission characteristics is such that they block the laser light and transmit harmonics in the wavelength range of roughly 15 nm–80 nm.

Experimental Procedure. Before generating higher order harmonics, some crucial experimental parameters of the setup need to be tested and checked.

- **Laser Parameters.** The Ti:Sapphire output needs to be characterized appropriately. This implies both temporal as well as spatial profile measurements, if possible at the position of interaction, i.e. inside the semi-infinite gas cell. Focusing should be arranged in such a way that peak intensities of about 1×10^{14} W/cm^2 are within reach, always guaranteeing that the damage threshold of the input window is not exceeded. It should be emphasized that the characterization of the laser parameters is crucial for an accurate analysis of results.
- **Beam Propagation.** The optical alignment of the system is, as always, important and crucial for repeatable results. Several apertures along the beam propagation path can be used as guiding reference points. The two most important reference points of the system are the pinhole at the exit of the generation chamber and the slit at the input of the analyzer chamber. As these two points define the optical axis of the system, it needs to be ensured that the chambers are mounted on the optical table so that their relative position does not change. Furthermore, a beam block should be placed behind the diffraction grating to block the zeroth order during actual measurement runs. This serves to protect the MCP from residual IR light. The optical alignment should be done with either an alignment laser (HeNe) or with the Ti:Sapphire output strongly attenuated.
- **Vacuum Parameters.** Before measurements can be made, it needs to be ensured that the necessary vacuum conditions are reached in the system. The most stringent requirement is given by the MCP in the analyzer chamber. It should only be switched on and operated if a pressure of $<5 \times 10^{-6}$ mbar is reached. This holds, in particular, for when the generation chamber is filled with rare gas, i.e. under load.
  A vacuum test should be performed as follows: Pump all chambers simultaneously with the scroll pump and open all valves between the respective chambers. Switch on the turbo pump in the analyzer chamber and monitor the pressure. When an equilibrium pressure is reached in the analyzer chamber, close the valve between the scroll pump and the generation chamber. Using a needle valve, slowly insert rare gas into the generation chamber while monitoring the pressure in the analyzer chamber. Note the maximum pressure in the generation chamber that allows for safe operation of the MCP in the analyzer chamber. Additional pumping apertures can be inserted along the beam propagation path to improve the pressure in the analyzer chamber. Note also that this pressure may be different for different rare gases. A detailed plan of the pumping scheme is given in Fig. 3.

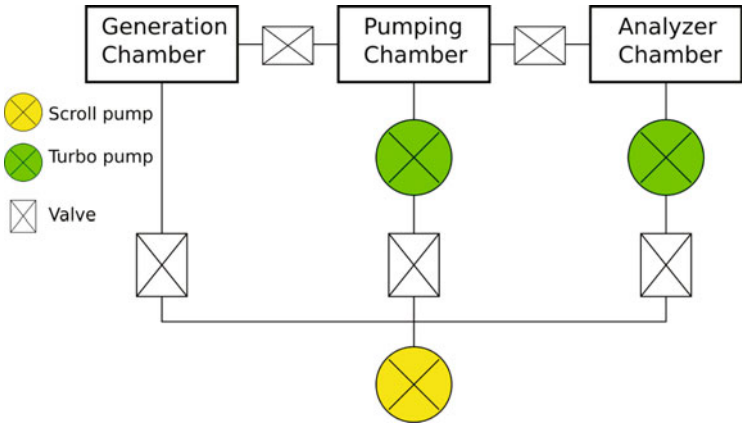

Fig. 3. Schematic of the pumping scheme (not to scale). The pumping chamber, not shown in Fig. 2 for clarity, serves as a differential pumping stage which is pumped with a turbo pump. In addition to the pinhole at the exit of the generation chamber, pumping apertures can be inserted between the respective chambers.

- **Detector System.** Once a sufficiently good vacuum has been created in the analyzer chamber, the detector system can be checked. The MCP is operated with high voltages (around 2 kV) so care has to be taken about all electrical connections made. The manual of the MCP contains the maximum voltage ratings as well as details on how to safely operate the device.

  An adjustable objective is mounted on the CCD camera so that the fluorescence signal can be imaged properly on the detector chip. To obtain the best resolution, it should be checked that the camera focuses on the screen of the MCP as opposed to, e.g., the output window. The camera needs to be securely mounted so that its position is fixed and a box should be placed around it so as to block stray light from the environment. When the MCP is running, a certain noise level should be seen on the camera even without any signal from the generation chamber.
- **XUV photodiode and amplifier.** The quantum efficiency of the XUV photodiode is known and tabulated by the manufacturer (Opto Diode Corp.). The manufacturer also provides a low-noise amplifier to detect few photons in the desired spectral range. This amplifier is to be calibrated in order to relate its voltage output to an optical input energy. An obvious option of doing this is by sending light of a laser at known frequency and known optical power in to relate the photodiode output to the input energy (see Sect. 4).
- **Spectrometer Calibration.** To understand interpret and measurement results, the spectrometer needs to be calibrated. It is useful to do the calibration as early as possible, e.g. with data of the first day. A straightforward approach to the calibration is a geometric one: The position of the zeroth order is related to the edge of the MCP and, considering the angle of incidence on the diffraction grating, it is calculated where harmonics orders should appear on the detector. Comparison with experimental data yields the calibration.

4 Experimental results

As stated in Sect. 2, the outcome of our HHG yield measurement should be related to the three parameters: laser intensity, gas pressure and propagation distance of the harmonics in neutral gas. To do so, energy measurements with the photodiode as well

as corresponding spectral measurements were acquired systematically for different combinations of gas pressure and laser intensity.

The propagation distance of the harmonics is generally altered by changing the distance of the focal position relative the the pinhole. Due to the relatively long Rayleigh range of about 5 mm using an f = 100 cm focal length lens, however, the harmonic output did not vary noticeably for a focal position change of ±5 mm. Thus, this quantity was kept constant throughout the measurement.

In what follows we report on the results of the experiment that we performed, according to the procedure described in Sect. 3 for the purpose of determining HHG brilliances for three different values of laser intensity and for two values of the gas pressure.

4.1 Determining the XUV photon number

As discussed in Sect. 3, we determine the yield of the HHG process by combining measurements with a calibrated XUV photodiode and the XUV spectrometer (see Fig. 2). The principle behind the combination of the two measurements and thus of the results for the HHG efficiency shall be briefly introduced in this section.

The calibration of the photodiode was achieved by sending the attenuated output of a Ti:Sapphire laser (see below) onto the photodiode and recording the output voltage of the photodiode amplifier as a function of the optical input energy. By considering the quantum efficiency of the photodiode as well as the photon energy at the given wavelength, we could relate the peak output voltage for a given amplifier setting to the total photo electron charge Q generated by the photodiode. Generally, this charge Q relates to the number of photons $\mathrm{N}(\omega)$ at frequency ω as

$$\mathrm{Q} = \mathrm{QE}(\omega) \cdot \mathrm{N}(\omega), \tag{1}$$

where $\mathrm{QE}(\omega)$ is the quantum efficiency at ω. It is characteristic for our experiment, however, that the XUV radiation incident on the photodiode is not monochromatic, as e.g. in the calibration of the XUV photodiode, but inherently broadband since we generate many harmonic orders of the fundamental frequency simultaneously. To calculate the yield and furthermore a brilliance (see below) of the HHG process, it is crucial to determine how many photons are in a given generated harmonic order. It follows that the contribution of each harmonic order to the total photo electron charge generated in the photodiode needs to be extracted from the measurements. To this end, it is instructive to mathematically relate the total charge Q to the photon number in a given harmonic q by considering Eq. (1):

$$\mathrm{Q} = \sum_q T\mathrm{f}_q \, \mathrm{QE}_q N_q. \tag{2}$$

Here, $T\mathrm{f}_q$ is the transmission value for harmonic q of the 500 nm aluminium filter and QE_q is the quantum efficiency of the photodiode at this wavelength. Furthermore, N_q is the photon number in a harmonic q. Since the photodiode measurement allows us to determine the total charge Q, we find the photon number N_q based upon the spectral measurement as follows. Assuming the quantum efficiency of the MCP detector in the spectrograph is constant over the investigated XUV spectral range [20], the number of photons N_q in harmonic order q can be related to the number of measured counts n_q in this particular harmonic by

$$N_q = \gamma \, \frac{n_q}{T\mathrm{f}_q R\mathrm{g}_q} = \gamma n_q^c, \tag{3}$$

where Rg_q is the gold grating diffraction in the spectrograph and n_q^c is the number of measured counts corrected for the filter transmission and grating diffraction. The gain factor γ accounts for the gain of the MCP and the collection efficiency of the CCD camera used to detect the output of the fluorescent back screen of the MCP detector.

From Eqs. (2) and (3) we observe that the only parameter which is not directly experimentally accessible is the gain factor γ. However, since it is a parameter inherent to the detection system, we can determine it by combining the photodiode measurements for Q and the spectral measurements for n_q, i.e. by combining the expressions in Eqs. (2) and (3). The number of photons in a given harmonic is then simply given by $N_q = \gamma \cdot n_q^c$.

4.2 Measurement results

After discussing how the photon number in a given harmonic order is retrieved from the measurements, the details as well as the results of these measurements shall be outlined in this section.

Characterization of laser parameters. The laser system used was an amplified Ti:Sapphire system operating at 20 Hz. The temporal duration of its pulses were measured to be 38 fs FWHM, using a second harmonic intensity autocorrelator. In order to compensate for the chirp introduced by optical elements in the beam path (BS, attenuating polarizer, focusing lens), the compressor length was adjusted for optimal harmonic yield. Furthermore, an iris was used to adjust the beam size for optimal harmonic output. For the used settings, the spot size in focus was measured to be 72 μm FWHM.

Spectral and photodiode measurements. The HHG spectra were acquired with the spectrograph using pulse energies in the fundamental of $E_p = 1\,\text{mJ}$, 1.2 mJ and 1.4 mJ. The lowest value corresponds to the threshold for our detection system while the highest was chosen in order to minimize the risk of pin-hole damage in case of accidental laser beam misalignement. Varying the pressure of our target gas, argon, between $P = 15\,\text{mbar}$, $P = 20\,\text{mbar}$ thus allowed us to perform HHG efficiency measurements for a combination of five different parameter sets (no measurement was taken with $E_p = 1.2\,\text{mJ}$ and $P = 15\,\text{mbar}$). Higher pressure values led to a reduction of the HHG detected signal in the chosen configuration, which we interpret as a consequence of the increase in absorption losses beyond the pin-hole in the pumping chamber. A typical spectrum acquired over 0.5 s, i.e. 10 laser shots, is shown in Fig. 4. The CCD (Andor) was operated in low noise mode (temperature $-60\,^\circ\text{C}$, read-out time $16\,\mu\text{s}$ per pixel, gain = 1). We note that without an aluminium filter single laser shot spectra could be acquired.

The HHG orders (horizontal coordinate in the detection plane) were determined by calibrating the spectrometer detector as described in Sect. 3. The calibration of the detector in terms of the divergence angle (vertical coordinate) was performed assuming the MCP to be positioned in the far field of the HHG source (the pin-hole) and taking into account the magnification of the MCP image on the CCD detector. With the given parameters we produce harmonic orders up to $q = 29$ which show a maximal divergence of about 2 mrad (see Fig. 4).

For the XUV pulse energy measurements, the photodiode was placed in the spectrograph chamber before the grating. These measurements were performed using an aluminium filter (Lebow) of 500 nm thickness. The amplifier used to amplify the photodiode signal was model PA-100 by Opto Diode Corp. With gain values of 500 and

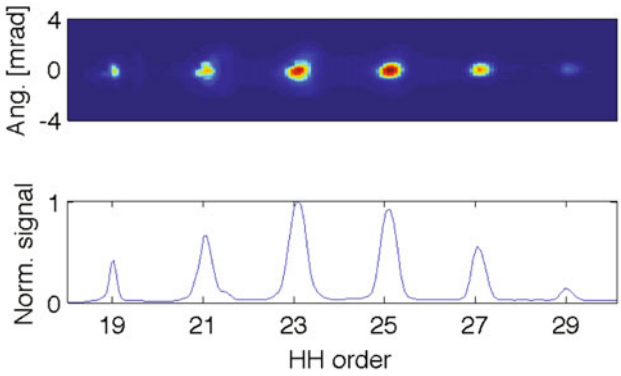

Fig. 4. Typical, measured HHG spectrum. The top shows the the angularly and spectrally resolved spectrum as detected on the CCD chip, the bottom the vertically integrated spectrum normalized to unity.

1000, the signal strength of the photodiode output was measured to be on the order of tens of mV, providing a sufficiently good signal to noise ratio. In order to account for small, shot to shot intensity fluctuations of the laser system we measured the photodiode output for 10 laser shots and averaged over these values.

Brilliance of HHG. As outlined in Sect. 4.1, the calculation of the gain factor γ in Eq. (3) is the first step in determining the efficiency of the HHG process with our setup. With the measurements as described above, we calculate a gain factor γ for each combination of target gas pressure and fundamental pulse energy. The mean result is $\gamma = 0.41$ which is the value used for the following efficiency calculation.

As our goal is to determine the efficiency and brilliance of the HHG process, it is important to define these terms precisely. They are:

$$\text{Brilliance} = \frac{\text{Number of XUV photons}}{\text{Laser shot} \cdot \text{Source area} \cdot \text{Solid angle} \cdot \text{Bandwidth of given harmonic}} \tag{4}$$

$$\text{Efficiency} = \frac{\text{Total XUV photon energy}}{\text{Input photon energy}}. \tag{5}$$

It is obvious that the brilliance is a quantity for each individual harmonic while the efficiency as defined above relates the total XUV output to the near-IR optical input. The source area can be well approximated by the area of the pinhole, giving a lower limit for the calculated efficiency. The bandwidth of each harmonic is the full bandwidth determined in the acquired spectra after calibration of the frequency axis. When compared to the brilliance definition used for synchrotron radiation, we replace the term 'per unit time' by 'per laser shot'. This is reasonable as we operated in a pulsed mode in which the actual duration of the XUV photon emission could not be determined accurately. For a quantitative comparison with synchrotrons, one should multiply the brilliance values obtained here with the laser repetition rate.

Evaluating our measurements with the spectrograph as well as the photodiode and using Eqs. (2) and (3), we find that we produced on the order of 10^5 photons in the brightest harmonics. This leads to peak brilliances of about 10^{-4} photons/laser shot/mm^2/mrad/BW, where BW is the bandwidth of a given harmonic in Hertz, and a maximum conversion efficiency of 1.2×10^{-8}. Our results for the brightest harmonics in each measurement and overall conversion efficiencies are summarized in Fig. 5.

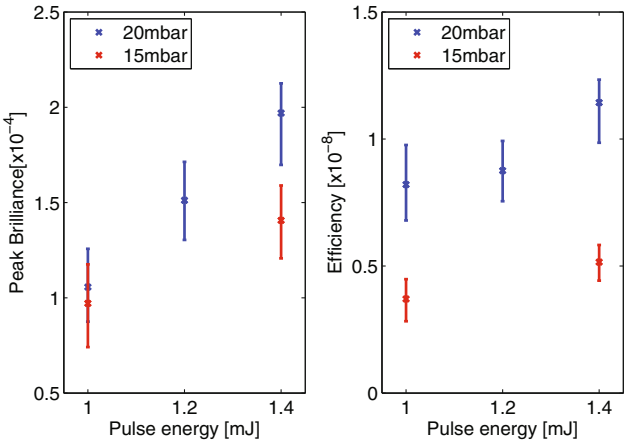

Fig. 5. Left: peak brilliance of each measurement, measured in photons/laser shot/ mm^2/mrad/BW. Right: HHG conversion efficiencies as defined in the text.

The results in Fig. 5 are grouped by color according to the target pressure used. We find that photon number, brilliance and efficiency of the HHG process increase with input energy of the fundamental pulse, while the increased target pressure of 20 mbar provides a positive 'offset' for these curves relative to the measurements at 15 mbar.

It is interesting to note that the peak brilliances at different pressures are measured for different harmonic orders. At 15 mbar target pressure, harmonic $q = 19$ shows the highest brilliance whereas harmonic $q = 21$ has the maximal brilliance value in the measurements at 20 mbar target pressure. We attribute this effect to phase matching mechanisms that lead to a better phase matching of a particular harmonic order at a given pressure (see discussion in Sect. 2).

The overall maximal conversion efficiency of 1.2×10^{-8} is certainly not the highest reported for HHG [18]. However, considering that no attempts for yield enhancement, such as quasi phase matching, were made, this result represents the inherent efficiency of our setup with a semi-infinite gas cell. The measurement provides a new data point in a scarse set of measurements on HHG efficiency and can thus serve the community to further advance with respect to higher yields.

Summary and outlook. We performed an efficiency measurement of the HHG process in a semi-infinite gas cell with respect to the two crucial parameters target gas pressure and energy in the fundamental pulse. Combining spectral measurements with an XUV spectrometer and energy measurements with a calibrated photodiode allowed us to determine a peak conversion efficiency of 1.2×10^{-8} while a peak brilliance for a single harmonic order of 2×10^{-4} photons/laser shot/mm^2/mrad/BW was detected.

The measurement technique proved to be reliable and straightforward to implement, suggesting that it allows to properly characterise many more HHG setups. For the given setup it would be of interest to investigate how a different focusing geometry as well as different target gases might affect the efficiency results.

References

1. A. McPherson, et al., J. Opt. Soc. America B **4**, 595 (1987)
2. M. Ferray, et al., J. Phys. B: Atom. Mol. and Opt. Phys. **21**, L31 (1988)
3. X. Li, et al., Phys. Rev. A **39**, 5751 (1989)

4. P. Corkum, Phys. Rev. Lett. **71**, 1994 (1993)
5. K.C. Kulander, et al., *Super Intense Laser Atom Physics (SILAP) III*, edited by B. Piraux (Plenum Press, New York, 1994)
6. G. Vaillancourt, et al., Opt. Lett. **15**, 317 (1990)
7. P.M. Paul, et al., Science (New York, NY) **292**, 1689 (2001)
8. M. Drescher, et al., Nature **419**, 803 (2002)
9. P. Agostini, et al., Rep. Prog. Phys. **67**, 813 (2004)
10. P.B. Corkum, et al., Nat. Phys. **3**, 381 (2007)
11. P. Agostini, et al., Contem. Phys. **49**, 179 (2008)
12. F. Krausz, et al., Rev. Mod. Phys. **81**, 163 (2009)
13. M. Lewenstein, et al., Phys. Rev. A **49**, 2117 (1994)
14. M. Lewenstein, et al., Phys. Rev. A **52**, 4747 (1995)
15. Z. Zeng, et al., Phys. Scr. **66**, 321 (2002)
16. D. Hum, et al., Comptes Rendus Physique **8**, 180 (2007)
17. C. Durfee, et al., Phys. Rev. Lett. **83**, 2187 (1999)
18. T. Popmintchev, et al., Proc. Nat. Acad. Sci. USA **106**, 10516 (2009)
19. J. Peatross, et al., J. Mod. Opt. **51**, 2675 (2004)
20. Correspondence with Hamamatsu